Surfaces and Interfaces 37 (2023) 102736

Contents lists available at ScienceDirect

Surfaces and Interfaces

journal homepage: www.sciencedirect.com/journal/surfaces-and-interfaces

Size- and temperature-dependent thermal transport across a Cu−diamond interface: Non-equilibrium molecular dynamics simulations

Hai Huang [a,b,*], Yinghui Zhong [a,b], Bin Cai [a,b], Jiefang Wang [a,b], Zhongxia Liu [a,b], Qing Peng [c,*]

[a] Key Laboratory of Material Physics of Ministry of Education, School of Physics and Microelectronics, Zhengzhou University, Zhengzhou 450052, China
[b] Institute of Intelligent Sensing, Zhengzhou University, Zhengzhou 450001, China
[c] State Key Laboratory of Nonlinear Mechanics, Institute of Mechanics, Chinese Academy of Sciences, Beijing, 100190, China

ARTICLE INFO

Keywords:
Interfacial thermal transport
Cu−diamond composites
Size effects
Temperature effects
Non-equilibrium molecular dynamics

ABSTRACT

Cu−diamond composites (CDCs) have greatly promising applications in thermal management for high-power electronics because of their outstanding thermophysical properties. Nonetheless, many fundamental mechanisms of interfacial thermal transport for CDCs remain poorly understood at present. Here we focus on investigating the size- and temperature-dependent thermal transport across a Cu−diamond interface using non-equilibrium molecular dynamics simulations. Results show that interfacial thermal conductance (ITC) is proportional to both the system size and ambient temperature. Especially, our predicted room-temperature ITC of 41.12 $MW{\cdot}m^{-2}{\cdot}K^{-1}$ at an infinitely long system is close to that of the experiments after an interface optimization. Additionally, the ITC at the system with a length of 323.2 Å is increased by over 2.5 times in the temperature range of 100−500 K, up to 36.39 $MW{\cdot}\ m^{-2}{\cdot}\ K^{-1}$. Detailed analyses of interfacial disorder and its concomitant effects, related to system size and temperature, are implemented for helping understand the significant improvement of ITC. The underlying mechanism is further uncovered by the phonon density of states as well as the spectral overlap factor at interfacial Cu and diamond. This study provides an important insight into the understanding of interfacial thermal transport in CDCs and a guideline for optimizing the design of CDCs in experiments.

1. Introduction

As power electronics technology moves toward miniaturization and functional integration, effective thermal management strategies urgently need to be proposed to tackle the significant improvement in volumetric power density [1–4]. Materials with high thermal conductivity (TC), as well as a close coefficient of thermal expansion (CTE) to that of the ceramic substrate or chip, offer feasible solutions to the thermal management design of high-power electronic devices [5,6]. In recent years, Cu−diamond composites (CDCs) have been considered as one of the most promising thermal management materials and are expected to be employed in the above harsh scenarios because of their outstanding thermophysical properties in theory, such as high TC, high working temperature, and tunable CTE [5–7].

In practice, however, the poor chemical affinity (*e.g.*, the contact angle up to 131.5° at the sintering temperature of 1473 K [8]) and the steep Debye temperature gradient between the Cu and the diamond greatly reduce the efficiency of thermal transport across their interfaces, causing the actual TC of CDCs far below the theoretical value [4–8]. Toward the purpose of achieving superior TC for the composites, the scientific community in materials has gradually attempted different preparation processes (including matrix alloying and diamond surface metallization, *etc*.) to enhance the interface bonding force [4–8]. Despite some improvement in the TC of CDCs due to the efforts, the experimental results are still too low. Empirically speaking, a prior understanding of the correlation between the atomic-level structure of a Cu−diamond interface (CDI) and its thermal transport behavior is, therefore, necessary to promote the optimization of interfacial thermal conductance (ITC) in experiments [9,10]. Several recent advances in atomistic studies of CDCs have provided some insights into understanding how the interfacial atomic structure, work of adhesion, and binding characteristics depend on the CDI stacking configuration with or without alloying elements and then affect the subsequent ITC [11–14]. Nevertheless, to the best of our knowledge, the atomic-level studies on thermal transport across a CDI are still in its infancy, and even many fundamental aspects remain unknown. For example, the investigation

* Corresponding authors.
E-mail addresses: huanghai@zzu.edu.cn (H. Huang), pengqing@imech.ac.cn (Q. Peng).

https://doi.org/10.1016/j.surfin.2023.102736
Received 28 November 2022; Received in revised form 11 January 2023; Accepted 4 February 2023
Available online 7 February 2023

paid general attention that ITC strongly depends on system size [15–19], is lack for the composites. Furthermore, phonons, because of the attribute of quantized lattice vibrations store, act as the major thermal carriers in dielectric and at metal−dielectric interfaces, and their transport characteristics are closely related to ambient temperature [16,20-22]. But unfortunately, the dependence of the interfacial phonon transport of CDCs on ambient temperature is not well understood yet.

So far, molecular dynamics (MD) simulations have been widely applied in the thermal physics of nanoscale materials and made great progress in the full prediction of phonon modal ITC with millions or tens of millions of atoms [15–22], profitably complementing both theoretical and experimental methods. Generally, there are two approaches to investigate thermal transport in MD, *i.e.*, the equilibrium MD (EMD) method based on the Green-Kubo formula and the non-equilibrium MD (NEMD) method derived from Fourier's law, respectively [16,23]. Among them, the NEMD method is more appropriate to compute the thermophysical properties of heterogeneous or polycrystalline systems since it is more like the measurements of TC in experiments [15-20,24, 25]. In this method, an axial temperature gradient across the mimic system is artificially generated first, and then the axial TC and ITC can be obtained owing to heat flux in the direction dependent on the temperature gradient [23,25,26]. In fact, NEMD, proposed by Chantrenne et al. [26], has been used to calculate TC in nanostructured materials when it came out. In the decades following that, many studies have adhered to the principle to simulate the thermal transport of nanoscale systems and compute the TC between dissimilar materials or across grain boundaries [15-20,22,24]. Therefore, in the present work, the NEMD method is adopted to investigate the interfacial thermal transport behaviors of CDCs from an atomistic insight. The effects of system size as well as ambient temperature on the interfacial thermal transport of the composites are described emphatically.

2. Simulation methodology

All simulations were performed using the Large scale Atomic/Molecular Massively Parallel Simulator (LAMMPS) package [27], and the atomistic visualizations were implemented with Open Visualization Tool (OVITO) software [28]. To study the interfacial thermal transport, a lamellar Cu(001)−diamond(001) model with the *xy* plane of 37.8 Å × 37.8 Å was initially created. The stacking mode was utilized because it has been proven by previous DFT studies to be the most stable structure [14]. The interface was built by adjusting the relaxed Cu (001) plane to match the fixed diamond (001) plane due to the hardness of diamond and the ductility of copper [14,29]. The interactions between Cu atoms, the interactions among C atoms in diamond, and the Cu–C interactions were described by the embedded atom method (EAM) potential [30], the Tersoff potential [31], and the Lennard-Jones potential [32], respectively. Among them, the reason for adopting the Tersoff potential to simulate the diamond is that the potential has been widely applied in the calculation of the thermal conductivity of carbon-based materials including diamond [25,33–35] and the MD results based on it is very close to the DFT and experimental measurement values [35]. To release the stress out of the CDI structure, a conjugate gradient minimization method under zero external pressure was carried out. Periodic boundary conditions along the three dimensions were applied in all calculations. The obtained ground state model is exhibited in Fig. 1(a). Before generating heat flux, the system was relaxed with the Nose-Hoover thermostat-barostat (NPT) ensemble under zero pressure at a constant temperature for 0.1 ns until reaching enough stable state. To examine the influence of system size on ITC, the length of simulation cell in the *z*-direction was set as 215.5, 323.2, 430.9, 538.6, or 646.4 Å, respectively, and the thermostat temperature was regulated to be 300 K. When investigating the temperature-dependent ITC, the temperature was maintained at 100, 200, 300, 400, or 500 K, respectively, while the *z*-direction length was determined to be 323.2 Å.

Subsequently, the outer layer with approximately 3.0 Å thickness along the *z*-axis of the simulation cell was fixed to disrupt the periodicity of this direction, and then a pair of heat reservoirs, each 15.0 Å thickness adjacent to the corresponding fixed layer, was started to produce a constant heat flux of 5.6 × 10^9 W· m^{-2} (see Fig. 1(b)). The heat was constantly poured into the reservoir on the side of Cu (*i.e.*, heat source), followed to one-dimensionally dissipate throughout the system, and eventually discharged into the reservoir located in the diamond region (*i.e.*, heat sink). During this process, atoms within the observed region were allowed to move adiabatically using the NVE ensemble (constant number of atoms, volume, and energy), and temperature controls in the heat reservoirs were realized by the Langevin thermostat. After lasting for 0.2 ns to achieve system stability, another 4 ns was run to collect the time-averaged temperature. The temperature profile was plotted by recording the local temperatures within each divided layer of 10.8 Å thickness along the *z*-axis in the observed region, from which the efficiency of thermal transport across the CDI was further evaluated. In all calculations, the heat flux was consistently carried out. Note that the simulated heat flux is larger than that of the actual situation and facilitates the formation of a distinct temperature gradient across the CDI for subsequent analysis, which agrees with the setting in other similar

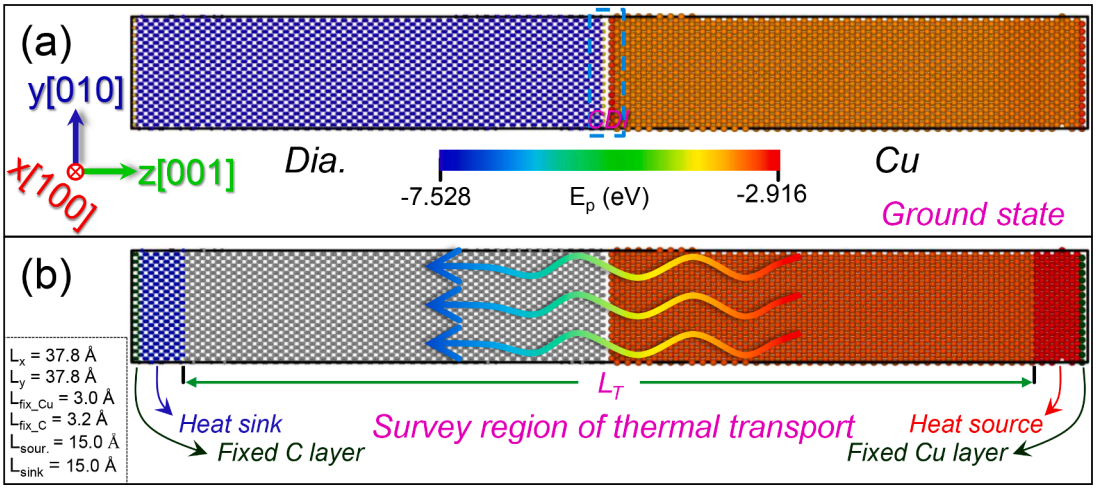

Fig. 1. NEMD simulation model and settings for the calculations of thermal transport across a CDI. (**a**) Schematic diagram of a CDI simulation cell at its ground state, in which the atomic potential energy distribution is exhibited. (**b**) Graphical interpretation of the system domain settings for NEMD simulation. The fixed layers, the heat source layer, and the heat sink layer are specified, respectively.

studies [36,37].

3. Results and discussion

3.1. General analysis of thermal transport

To briefly describe the interfacial thermal transport behaviors of CDCs, it is appropriate to choose one of a series of results to expound [38]. As an example, the system with a *z*-direction length of 323.2 Å at 300 K is investigated, and its time-averaged temperature profile along the *z*-axis at different periods is shown in Fig. 2. Note that local temperature within a divided layer of the system is calculated by the atomic kinetic energy as follows [16]

$$T_i = \frac{1}{3N_n k_b}\sum_{j=1}^{N_i} m_j V_j^2, \quad (1)$$

where k_b is the Boltzmann constant, and N_i, m_j, and V_j represent the number of atoms in the i^{th} divided layer and the mass and velocity of j^{th} atom in the layer, respectively. The time-averaged temperature data was extracted over every 0.5 ns period, and this operation finished after 4.0 ns since the stabilization in all the local temperatures has been achieved before the moment. Over time, the temperature is gradually raising on the side of Cu bulk, while a downtrend occurs on the side of diamond bulk. After every 0.5 ns, both the increasing amplitude of temperature on the side of Cu bulk and the falling amplitude on the side of diamond bulk present a decline. These suggest that an ordered temperature field or a heat dissipation channel has been established step by step. The temperature gradient becomes steeper and steeper on the side of Cu bulk, whereas almost no change on the side of diamond bulk. The slope of the former is also significantly greater than that of the latter (close to zero), originating from the huge differences in TC between diamond (up to 2200 $W\cdot m^{-1}\cdot K^{-1}$ [39]) and Cu (approximately 400 $W\cdot m^{-1}\cdot K^{-1}$ [40]). The high TC facilitates the uniform distribution of temperature fields within the diamond bulk in a very short time. Exceptionally, the local temperature of the diamond near the interface gradually deviates from that of its bulk after 2.0 ns and the deviation exceeds 10 K at 4.0 ns. This could be because the slightly interfacial disorder after sufficiently thermal relaxation occurs but improves the contact on both sides of the interface to facilitate heat dissipation from the Cu to the diamond. At 4.0 ns, through linearly fitting the temperature profile extrapolated from the bulk to the interface, the time-averaged temperature jump at the interface can be calibrated and reaches approximately 220.3 K. On this basis, the ITC (G_{int}), *viz.*, the reciprocal of the Kapitza resistance or interfacial thermal resistance (R_{int}), can be obtained according to Fourier's law as follows [36]

$$G_{int} = \frac{1}{R_{int}} = \frac{J}{\Delta T_{int}}, \quad (2)$$

where J and ΔT_{int} denote the heat flux and the temperature jump at the interface, respectively. Ultimately, the stable G_{int} at 300 K is determined as 25.42 $MW\cdot m^{-2}\cdot K^{-1}$, numerically comparable to the results of Chen et al. [12] using first-principles calculations for three different Cu(111)–diamond(111) stacking configurations (*i.e.*, 18.5 – 26.9 $MW\cdot m^{-2}\cdot K^{-1}$). However, the calculation is nearly an order of magnitude lower than those of the Cu–Si system [36]. This may be due to a significantly greater difference in the TC between Cu and diamond than that between Cu and Si (approximately 142 $W\cdot m^{-1}\cdot K^{-1}$ [41]), causing an inflexible interfacial thermal transport. In addition, the temperature drops, both in Cu bulk and diamond bulk, are significantly small relative to the ΔT_{int}, indicating that the thermal resistance of CDCs is determined by the ΔT_{int}. Therefore, it is of great significance to reduce the ΔT_{int} for improving the capability of thermal conduction of CDCs.

Generally, the mechanisms of interfacial thermal transport can be spied indirectly from the perspective of the phonon density of states (PDOS), since the PDOS can quantify the change in phonon spectrum originating from the vibrational mismatches between different crystal structures in contact across an interface [38,42,43]. The PDOS is computed by performing the fast Fourier transform of the atomic velocity autocorrelation function (VACF) from the MD simulations as follows [44,45]

$$PDOS(\omega) = \int_{-\infty}^{\infty} e^{-i\omega t} VACF(t)dt, \quad (3)$$

where

$$VACF(t) = \frac{1}{N}\sum_{j=1}^{N} < v_j(0)v_j(t) >. \quad (4)$$

Here ω is the vibration frequency of phonon, N is the number of atoms in an examined region, $v_j(t)$ refers to the velocity vector for j^{th} atom at time t, and ⟨…⟩ denotes the ensemble average, respectively. To further quantify the PDOS mismatch at the interface, the overlap factor S can be defined as follows [45]

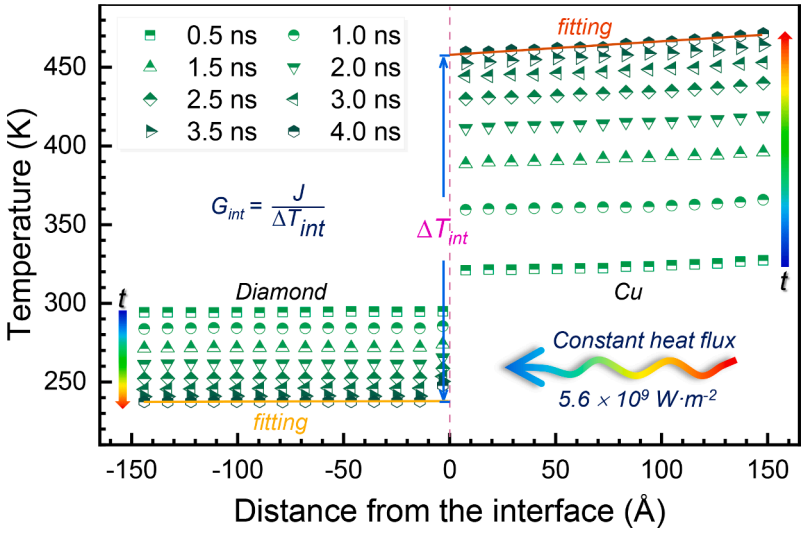

Fig. 2. A typical temperature profile *versus* distance away from the interface at different times for the CDI system with a length of 323.2 Å at 300 K. The temperature data was extracted over every 0.5 ns period, lasting for 4.0 ns.

$$S = \int_{-\infty}^{\infty} \min\{P_X(\omega), P_Y(\omega)\}d\omega, \quad (5)$$

where $P_X(\omega)$ and $P_Y(\omega)$ represent the PDOS of two different materials on both sides of the interface region, respectively. In fact, many studies have demonstrated that the ITC is strongly associated with the overlap factor, and a high overlap of spectra often means strong phonon coupling that facilitates thermal transport across the interface [36,45,46]. It is worth noting that there is no consensus as to whether Cu electrons can transfer energy to the dielectric directly although they can participate in interfacial thermal transport via electron-phonon coupling [36]. Hence, we focus on the phonon-interfacial transport for the CDCs hereinafter.

Because of the atoms at the physical interface normally behaving distinct characters from those in their bulk, a derived interface between the physical interface and the corresponding bulk in each material will inevitably arise [29,36]. As for the CDCs, the identification of atoms in different regions, including the bulk Cu atoms (Cu_{bulk}), the interfacial Cu atoms (Cu_{int}), the interfacial C atoms (Dia_{int}), and the bulk C atoms (Dia_{bulk}), has been described in our previous study [47]. Hence, a total of three interfaces are in the model system in principle and involve Cu_{bulk}–Cu_{int}, Cu_{int}–Dia_{int}, and Dia_{int}–Dia_{bulk} interfaces, each with their corresponding ITC (see Fig. 3(a)). To illustrate the interfacial phonon coupling, the PDOS of the final state as a function of frequency is computed for the four regions and exhibited in Figs. 3(*b*–*d*). The PDOS spectra show that the phonon modes are dominated by low frequencies for the Cu in nature, varying from 0 to 10.0 THz, while they are in a high-frequency domain (ranging from 10 to 50 THz) in the diamond. Due to the difference in interfacial structures, the overlap factor varies with changes in the interface combinations. The degree of overlap shows the largest for the Cu_{bulk}–Cu_{int} interface, followed by that of the Dia_{int}–Dia_{bulk} interface, and the smallest for the Cu_{int}–Dia_{int} interface. These can further give the following hints. First, taking the corresponding Cu or diamond bulk as a reference respectively, the C atoms present a relatively larger lattice disturbance than that of Cu atoms at the CDI (also mentioned in Fig. 2), ultimately causing intense phonon scattering at the Dia_{int}–Dia_{bulk} interface reducing the overlap factor. Next, the phonon scattering at the Dia_{int}–Dia_{bulk} interface triggers the predominant frequency domain from a low band slightly shifting to a high band (see Fig. 3(d)), while almost no change for the predominant frequency domain at the interfacial Cu region relative to the Cu bulk because of a good lattice order (see Fig. 3(b)). Given that the low-frequency phonons transport thermal energy more efficiently [48], the shift of the frequency domain for the inside of the diamond indicates a reduction of the transmission efficiency of extended phonons and impedes thermal transport. This also can explain why the slight temperature jump occurs at the Dia_{int}–Dia_{bulk} interface after the relaxation of 4 ns (see Fig. 2). Finally, the frequency domains between the Cu bulk and the diamond bulk hardly overlap, implying that the two materials are inherently incompatible for heat transfer. However, the slightly interfacial disorder due to the diamond provides additional phonon modes, reflected in the broadening in the frequency spectrum of the diamond. This facilitates the phonon coupling of the CDI (see Fig. 3(c)) and thus brings in new anharmonic channels. With the help of these channels, phonons have a high probability of transmitting to the other side, which can lower the thermal resistance. Taken together, the lattice disturbance of the interfacial diamond causes a negative effect on the phonon transport of its bulk and a positive effect on that of CDI, respectively. This highlights the necessity of the strategies proposed at present for the interface material design of thermal management [4,6], such as the interface modification with carbide or with defects, providing an effective heat dissipation channel that can enhance the positive effect but restraint the negative effect. In addition, thanks to the significant large overlap factor of CDI, the thermal resistance of the Cu_{bulk}–Cu_{int} or Dia_{int}–Dia_{bulk} interface is typically negligible compared to that of the physical interface between two materials (*viz.*, Cu_{int}–Dia_{int} interface) [36]. Thus, the following focuses solely on discussing the

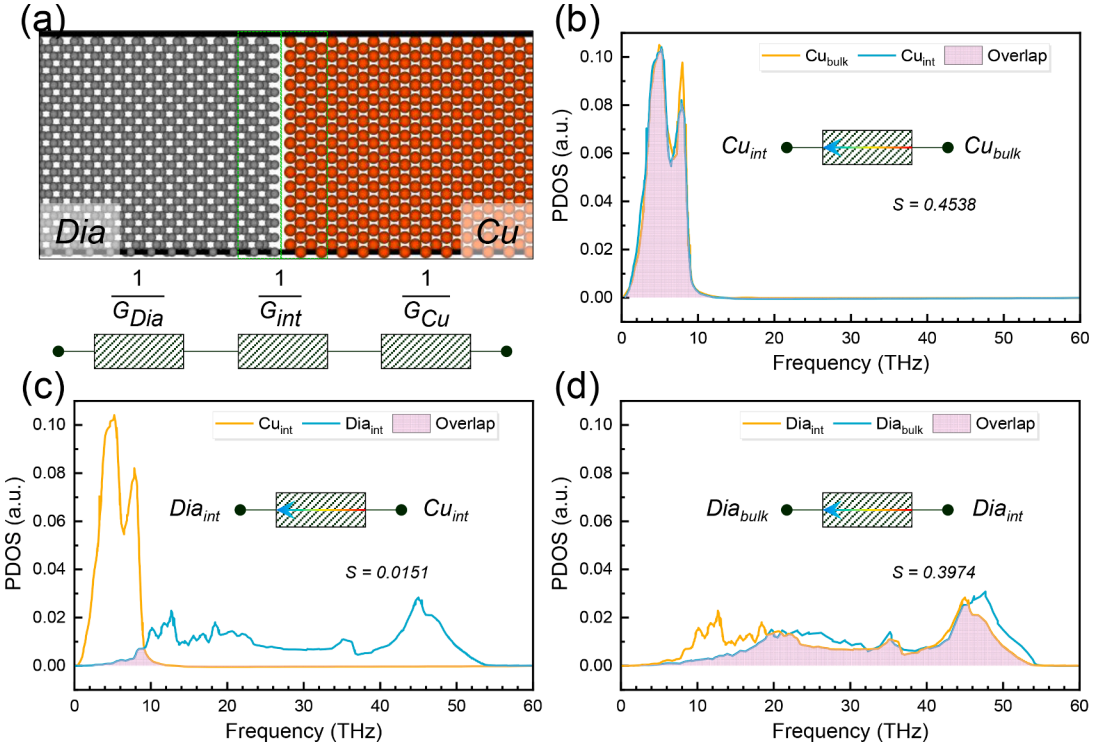

Fig. 3. Different atomic regions near a CDI and corresponding PDOS spectra. (**a**) Illustration of three interfacial regions and their thermal resistances, including a CDI (*i.e.*, Cu_{int}–Dia_{int} interface) and two derived interfaces (*i.e.*, Cu_{bulk}–Cu_{int} and Dia_{int}–Dia_{bulk} interfaces). (**b**) PDOS spectra for Cu_{bulk}–Cu_{int} interface. (**c**) PDOS spectra for Cu_{int}–Dia_{int} interface. (**d**) PDOS spectra for Dia_{int}–Dia_{bulk} interface. The overlap factors are given in the panels (*b* – *d*).

thermal transport across the Cu_{int}−Dia_{int} interface or CDI.

3.2. System size effects on thermal transport

As the characteristic size of a system is close to the phonon mean free path (MFP), the ballistic phonon transport becomes dominant in the simulation system because of the inadequate phonon–phonon scattering and the internal reflections of phonons from the boundaries [17,49,50]. As for NEMD simulations, heat reservoirs also may affect the propagation of ballistic phonons by boundary scattering so that the TC changes significantly with the decrease of system size [17,51]. For this reason, the ITCs of the CDI system with different *z*-direction lengths (L) ranging from 215.5 to 646.4 Å at 300 K are calculated, as shown in Fig. 4(a). The interfacial thermal resistance presents a positive correlation with the reciprocal of the L. In other words, the ITC monotonically increases (from 24.33 to 35.64 MW· m^{-2}· K^{-1}) with the increasing L, consistent with those observed in other interface-related materials [16,18,48]. As proposed by Yang et al. [17], the ITC of an interfacial system with infinite length can be obtained roughly from its corresponding system with finite size by extrapolation of a straight linear fit as follows (*viz.*, the analog of Matthiessen's rule [50])

$$\frac{1}{G_{int}(\infty)} = \frac{1}{G_{int}(L)} + \frac{K}{L}, \tag{6}$$

where $G_{int}(\infty)$ is the ITC of an infinitely long system, and K denotes a constant related to the $G_{int}(\infty)$ and phonon MFP. When the L approaches ∞, the theoretical value of ITC is computed as 41.12 MW· m^{-2}· K^{-1}, which is even close to the optimum result (45.30 MW· m^{-2}· K^{-1}) of the experimental calculations on the CDI modified by a WC layer [7]. This indicates that the interface optimization technology at present is still far from perfect for improving the ITC of CDCs, and the potential is substantial in the future. Further, for a bilayer structure, the associated relationships between its overall TC and partial ITC can be established by the formula based on a rule of mixtures as follows [52]

$$\kappa = \frac{L}{L_X}\kappa_X + \frac{L}{L_Y}\kappa_Y + LG_{int}, \tag{7}$$

where L_X and L_Y represent the lengths of two different materials on both sides of an interface, and κ_X and κ_Y are the TC of pure counterparts of the two materials, respectively. Herein, both the Cu and diamond layers are approximately half the total length of the simulation system in all cases. Combined with the linear formula fitted in Fig. 4(a), Eq. (7) can be reduced to the following expression

$$\kappa = p + qL, \tag{8}$$

where p denotes the $G_{int}(\infty)$, and q is a constant related to the TCs of pure Cu and pure diamond. Thus, like the ITC, the overall TC of the CDI system is also linearly proportional to the L at a certain temperature, *i.e.*, the longer the system size, the higher the TC, showing excellent conformity with prior studies on other nanolaminate composites [48,53]. In general, the interatomic distances exhibit a slight contraction or expansion (*i.e.*, strain contrast) near an interface relative to those away from the interface, causing a disorder of interface. In addition to the kinetic energy of the system being altered, the disorder may also affect the potential energy by regulating the elastic constants of associated atomic linkages of the interface [54]. As a result, when traversing the interface, a thermal carrier gets scattered, which eventually reduces the group velocity of phonons and localizes phonon modes around the disordered atoms of the interface [21]. Theoretically, it is detrimental to interfacial thermal transport for the presence of localized phonon modes [21]. Therefore, it can simply speculate that a shorter supercell has a higher proportion of interfacial atoms in the system (*viz.*, relatively more serious disorder in the interface but no more additional phonon modes provided) and then increases the phonon scattering probability, which is responsible for the lowering ITC.

To acquire a better intuition of the relationship of the ITC with the L,

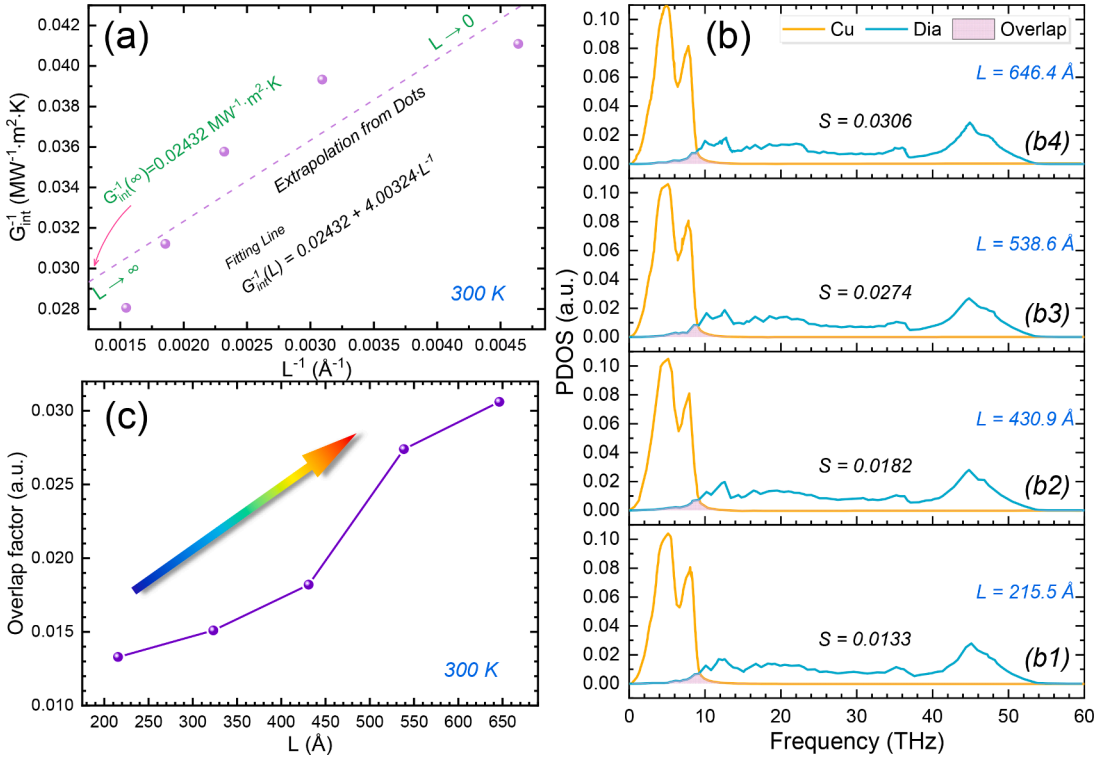

Fig. 4. Size-dependent thermal transport across a CDI at 300 K. (**a**) Interfacial thermal resistance *versus* the reciprocal of *z*-direction length. (**b**) Variation of PDOS spectra for a CDI with the length (ranging from 215.5 to 646.4 Å). Note that the PDOS spectra for the length of 323.2 Å have been given in Fig. 3(c). (**c**) PDOS overlap factor as a function of system length.

the PDOS spectra of both interfacial Cu and diamond regions are further calculated and shown in Fig. 4(b). As can be seen, both Cu- and diamond-predominant PDOS peaks present an increasing trend with the increase of L, particularly noticeable in the Cu (*e.g.*, rising from 0.104 to 0.110 at its first peak), indicating that the phonon scattering and boundary scattering are attenuated. Additionally, there is not a significant change for the full width at half-maximum of each peak in the PDOS profiles, implying that new anharmonic channels are not further opened. On the other hand, their dominant phonon modes are slightly shifted from high frequency to low frequency with the increasing L. For example, the phonon frequency at the first prominent peak of Cu gradually reduces from 5.13 to 4.94 THz, as the L is increased from 215.5 to 646.4 Å. The classical physical theory has shown that the phonon MFP has an inverse dependence on frequency [55]. Thus, the redshift means the increase of phonon MFP or the decrease of phonon energy. Generally, the thermal transport in solids also can be roughly understood from the simple phonon kinetic theory [15], in which the lattice thermal conductivity is defined as follows

$$\kappa = \frac{1}{3}\mathrm{Cvl}, \tag{9}$$

where C, v, and l represent the specific heat capacity of lattice, the group velocity of lattice waves, and the phonon MFP, respectively. Given that the specific heat capacity and the group velocity of phonons are essentially independent of system size [15], it can be deduced from Eq. (9), combined with Eqs. (6) and (8), that the increment of phonon MFPs facilitates the transmission of phonons across the CDI and then improves the ITC with the increasing L. In addition, the PDOS overlap factor is extracted from Fig. 4(b) and shown as a function of L in Fig. 4(c) to quantify the variation of ITC. The overlapping phonon frequency domain is mainly located between 6.0 and 10.0 THz. It can be seen that the overlap factor increases with the increase of L, which has a significant part of the contribution from the increase in the intensity of the diamond peak with the least frequency (around 10.0 THz). This reflects an enhancement of the capacity of exchange thermal energy at the CDI, showing a good agreement with the tendency of ITC.

3.3. Ambient temperature effects on thermal transport

Thermal transport at the nanoscale generally displays various temperature-dependent behaviors. At low temperatures, atomic vibrations are almost in a frozen state and keep that way until the ambient temperature is elevated to a proper level. At high temperatures, the nonlinear thermal flutter characteristics exhibit considerably and thus phonon anharmonicity raises rapidly, causing a decline in TC [56]. However, once the temperature exceeds the Debye limit, the group velocity of phonons is considered constant, and classical atomistic calculations are difficult to accurately evaluate the TC [56]. Usually, the TC is inversely proportional to ambient temperature in single atomic crystals (*e.g.*, graphene) at high temperatures [21,57,58], while a slowly diminishing characteristic of TC happens in some binary atomic structures (*e.g.*, GaN) with increasing temperature because of the almost overwhelming effects of their high-frequency phonons [59,60]. Hence, it is significantly crucial to disclose what types of temperature-dependent behaviors live in the CDI system for understanding its thermal transport.

Focusing on interfacial thermal transport, Fig. 5(a) shows the ITCs of the CDI system with a length of 323.2 Å in the temperature range from 100 to 500 K. Like the tendency in the case of L, the ITC exhibits a positive correlation with the ambient temperature. The ITC has a minimum value of 14.28 MW· m^{-2}· K^{-1} at 100 K and gradually raises to 36.39 MW· m^{-2}· K^{-1} at 500 K, increasing by over 2.5 times in the temperature range considered. A similar increase in ITC has also been observed in other interface-related systems disclosed in existing

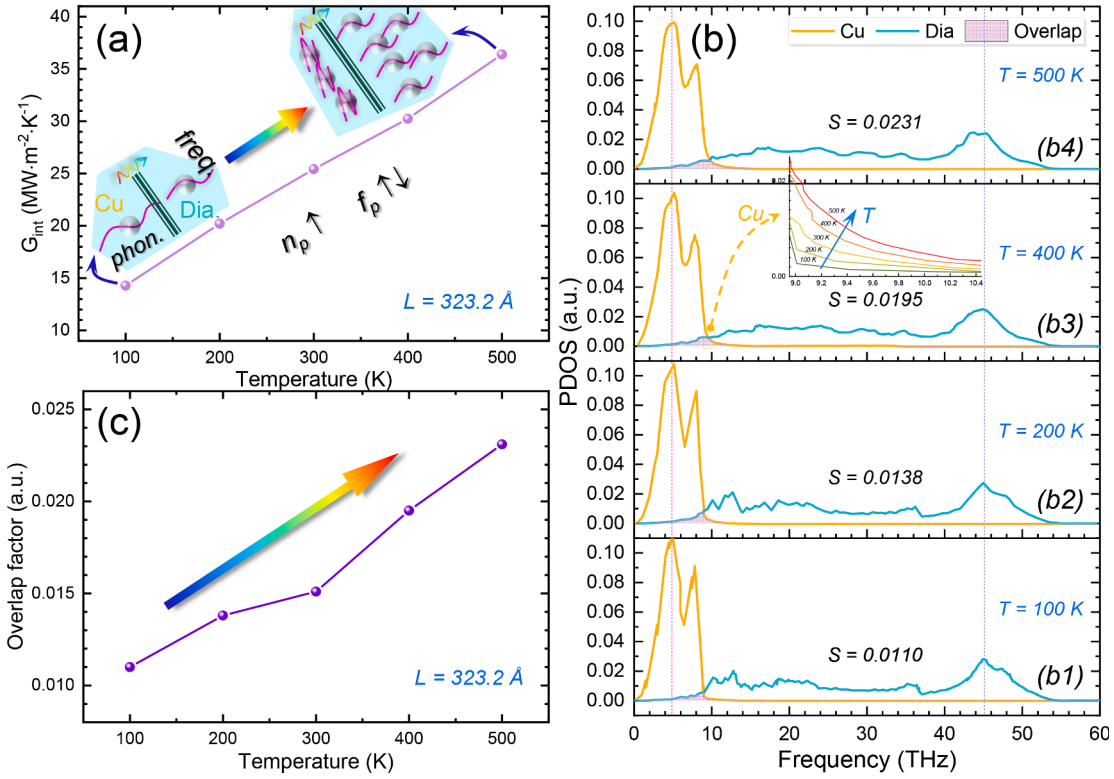

Fig. 5. Temperature-dependent thermal transport across a CDI in the system with a length of 323.2 Å. (**a**) ITC *versus* ambient temperature. A schematic illustration for changes in frequency and population of phonon traversing a CDI is displayed. (**b**) Variation of PDOS spectra for a CDI with temperature (ranging from 100 to 500 K). Each PDOS profile of Cu around 10 THz is magnified. Note that the PDOS spectra at 300 K have been given in Fig. 3(c). (**c**) PDOS overlap factor as a function of temperature.

literature [20,22,33,56,61,62], such as $Cr_{0.22}Ni_{0.78}-Al_2O_3$ and Al−graphene composites [20,61]. In addition, many studies on thermal interface materials have found that, unlike the case of L, the tendency of TC with temperature is often opposite of that of ITC [53,56,62-64], implying another connection between the two of them. For the issue of TC, it is widely believed by researchers to be caused by the Umklapp scattering or the inelastic scattering at elevated temperatures [21,56], especially the contribution from high-frequency phonons [21]. Analogically, this viewpoint could be introduced to explain the temperature dependence of ITC. At elevated temperatures, the processes of three-phonon scattering, including Normal and Umklapp (or U) scattering, are generally dominant [21,56,58]. Especially, Umklapp scattering can intensify the anharmonic interaction of phonon–phonon, causing the phonon momentum sum to point to the outside of the first Brillouin zone, and then resulting in phonon frequency modification [58]. Because of Umklapp scattering proportional to the square of frequency [21], the phonon frequency often improves with temperature. However, when encountering an interface, the high-frequency phonons are localized and have a high probability of splitting each into multiple low-frequency phonons at elevated temperatures [56,62], triggering an enhanced inelastic phonon–interface scattering that contributes to the redistribution of phonon frequency among different modes. For example, the peak intensity of phonons around 8.0 THz shows a decline in the interfacial Cu relative to Cu bulk at 300 K, while a peak broadening around 5.0 THz (see Fig. 3(b)), confirming the occurrence of the phonon-splitting processes near the CDI. In theory, there is a great chance for phonons with low frequency from one side of the interface to transmit to the other side relative to those with high frequency [56]. Consequently, an improvement in the coefficient of phonon transmission at the interface may occur. On the other hand, an increase in temperature excites more phonons, causing the further increase of anharmonic phonon–interface scattering probability. Therefore, the second modification of predominant phonon frequency (f_p) and the increase in the population of phonons (n_p) near the CDI at elevated temperatures facilitate better thermal transport across the interface (see the inset of Fig. 5(a)).

To further unravel the physical mechanisms of the temperature-dependent ITC, we also calculate the PDOS of both interfacial Cu and diamond regions, respectively, as shown in Fig. 5(b). Contrary to the scenario in L, there is significant damping in the peak intensity of the predominant PDOS in both Cu and diamond as the temperature rises, consistent with the tendency observed in other thermal interface materials [62,65]. For example, the highest peak of Cu phonon spectrum around 5.0 THz decreases from 0.112 to 0.099, and suppression from 0.028 to 0.025 around 45.0 THz for that of the diamond. Meanwhile, the proportion of PDOS in the broadly unimpressive frequency domain has a slight growth with the increasing temperature, such as that in the frequency range of 8.0−11.0 THz in the Cu (see the inset of Fig. 5(b)) or 15.0−40.0 THz in the diamond, indirectly causing the broadening of phonon modes in the PDOS profiles. On the other hand, the increasing temperature prompts a slight frequency shift from low to high on the side of Cu (*e.g.*, from 4.95 to 5.15 THz at its highest peak), while from high to low on the side of diamond (*e.g.*, from 45.0 to 43.7 THz at its highest peak), like the frequency shift of interfacial Si in the Si−Ge system [62]. The opposite frequency-shifting directions of the two imply that their PDOS profiles tend to overlap step by step with the increasing temperature. The pronounced redistribution of phonon modes may be attributed to the increased inelastic phonon–interface scattering at elevated temperatures. Generally, at an elevated temperature, the intensity of PDOS in the overall frequency domain could be suppressed because of the Umklapp scattering. But under the effects of increased anharmonic phonon–interface scattering at elevated temperatures, phonons with a higher frequency on one side of the interface may continuously scatter into the phonons with lower frequency [62], which can be further superimposed onto the pristine phonon spectrum and again initiate the change of phonon modes (*e.g.*, amplitude variation, broadening, and/or frequency shift), especially in the low-frequency domain. For the PDOS profile of Cu, its broadening of phonon modes may be more remarkable than that of diamond, since the predominant PDOS in the Cu is mainly located in its low-frequency domain. Consequently, this is beneficial to the improvement of the overlap of the spectra between Cu and diamond and carrying more thermal energy from the side of the Cu to the side of the diamond. To highlight the phonon transmission behavior, the PDOS overlap factor as a function of ambient temperature is further exhibited in Fig. 5(c). The overlap factor does increase with the increase of temperature, consistent with the tendency in ITC. Because of the overlap essentially located in a low-frequency domain, the acoustic phonons necessarily play a more important role in carrying thermal energy relative to the optical phonons for the CDCs [21]. There are usually three modes for the acoustic phonon, *i.e.*, the out-of-plane acoustic (ZA), transverse acoustic (TA), and longitudinal acoustic (LA) phonons [56]. Benefiting from high specific heat as well as large mean scattering time [43], the ZA phonons may make a dominant contribution to thermal transport across a CDI. In addition, the interfacial disorder may improve the contact on both sides of the interface and provide additional phonon modes, as mentioned in SubSection 3.1. The increasing temperature can intensify a rearrangement of CDI structure or interfacial disorder [47] and then facilitate the interfacial thermal transport, another possible interpretation for the improvement in overlap factor.

4. Conclusions

In this study, for a fundamental research purpose, we have performed an investigation of interfacial thermal transport behaviors for CDCs with different system sizes and ambient temperatures using NEMD simulations. The general results show that a slightly interfacial disorder due to thermal relaxation facilitates heat dissipation from the side of the Cu to the side of the diamond, originating from the strengthened contact on both sides of the interface. Especially, the disorder contributed by interfacial diamond may provide new anharmonic channels, improving the phonon transmission efficiency. With the increase of system size (215.5 − 646.4 Å), the ITC monotonically increases from 24.33 to 35.64 $MW\cdot m^{-2}\cdot K^{-1}$ at room temperature, and even the ideal result of 41.12 $MW\cdot m^{-2}\cdot K^{-1}$ at an infinitely long system is comparable to that of the experiments after an interface optimization. The tendency stems from the decrease of elastic scattering probability of phonons because of a relatively low proportion of interfacial atoms in the system as well as almost constant anharmonic channels. Intrinsically, a change in a system configuration with the increasing size causes the growth of the Cu- and diamond-predominant PDOS peaks and their frequencies shift from high to low, eventually resulting in an improvement in PDOS overlap factor that favors the capacity of exchange thermal energy at the CDI. On the other hand, as the ambient temperature rises from 100 to 500 K, the ITC also exhibits a positive response, increasing from 14.28 to 36.39 $MW\cdot m^{-2}\cdot K^{-1}$, benefiting from the intensification of interfacial rearrangement that can enrich additional phonon modes. The underlying reason for that is that an increased inelastic phonon–interface scattering at elevated temperatures, due to the second modification of predominant phonon frequency and the increase in the population of phonons near the CDI, has a significant impact on the redistribution of phonon modes (*e.g.*, amplitude variation, broadening, and/or frequency shift), which is beneficial to the improvement in PDOS overlap factor and carrying more thermal energy to transmit the interface. Overall, the ITC of CDCs strongly depends on its system size and ambient temperature. The current investigation significantly facilitates our understanding of the interfacial thermal transport in CDCs and provides a reference for assessing the thermophysical properties in experiments, contributing to promoting the application of the composites in thermal management for power electronics.

CRediT authorship contribution statement

Hai Huang: Conceptualization, Funding acquisition, Supervision, Software, Project administration, Writing – original draft, Validation. **Yinghui Zhong:** Data curation, Resources, Methodology. **Bin Cai:** Data curation, Investigation, Validation. **Jiefang Wang:** Data curation, Investigation, Validation. **Zhongxia Liu:** Data curation, Investigation, Validation. **Qing Peng:** Investigation, Methodology, Writing – review & editing.

Declaration of Competing Interest

The authors declare that they have no known competing financial interests or personal relationships that could have appeared to influence the work reported in this paper.

Data availability

Data will be made available on request.

Acknowledgments

This work was supported by the National Natural Science Foundation of China (Grant No. 12105249), the Key Project for Science and Technology Development of Henan Province (Grant No. 212102210195), the Innovation Team Support Program for Cooperation of Young Talents & Enterprises in Zhengzhou University (Grant No. 32320368), the Henan Province Postdoctoral Science Foundation (Grant No. 202102012), the Research and Practice Project of Education and Teaching Reform in Zhengzhou University (Grant No. 2022ZZUJG173), the State Key Laboratory of Nuclear Physics and Technology, Peking University (Grant No. NPT2021KFJ05), the Top Doctoral Talents Program of Zhengzhou University (Grant No. 21350621), and the National Supercomputing Center in Zhengzhou.

References

[1] K.A. Agbim, D.G. Pahinkar, S. Graham, Integration of jet impingement cooling with direct bonded copper substrates for power electronics thermal management, IEEE T. Comp. Pack. Man. 9 (2018) 226–234, https://doi.org/10.1109/TCPMT.2018.2863714.

[2] S. Sudhindra, F. Kargar, A.A. Balandin, Noncured graphene thermal interface materials for high-power electronics: minimizing the thermal contact resistance, Nanomaterials 11 (2021) 1699, https://doi.org/10.3390/nano11071699.

[3] G. Moreno, S. Narumanchi, X. Feng, P. Anschel, S. Myers, P. Keller, Electric-drive vehicle power electronics thermal management: current status, challenges, and future directions, J. Electron. Packaging 144 (2022), 011004, https://doi.org/10.1115/1.4049815.

[4] P. Zhu, P. Wang, P. Shao, X. Lin, Z. Xiu, Q. Zhang, E. Kobayashi, G. Wu, Research progress in interface modification and thermal conduction behavior of diamond/metal composites, Int. J. Min. Met. Mater. 29 (2022) 200–211, https://doi.org/10.1007/s12613-021-2339-6.

[5] J. Ma, L. Bolzoni, F. Yang, Interface manipulation and its effects on the resultant thermal conductivity of hot-forged copper/Ti-coated diamond composites, J. Alloy. Compd. 868 (2021), 159182, https://doi.org/10.1016/j.jallcom.2021.159182.

[6] S. Jia, F. Yang, High thermal conductive copper/diamond composites: state of the art, J. Mater. Sci. 56 (2021) 2241–2274, https://doi.org/10.1007/s10853-020-05443-3.

[7] J. Sang, Y. Yuan, W. Yang, J. Zhu, L. Fu, D. Li, L. Zhou, Exploring the underlying causes of optimizing thermal conductivity of copper/diamond composites by interface thickness, J. Alloy. Compd. 891 (2022), 161777, https://doi.org/10.1016/j.jallcom.2021.161777.

[8] J. Sang, L. Zhou, W. Yang, J. Zhu, L. Fu, D. Li, Enhanced thermal conductivity of copper/diamond composites by fine-regulating microstructure of interfacial tungsten buffer layer, J. Alloy. Compd. 856 (2021), 157440, https://doi.org/10.1016/j.jallcom.2020.157440.

[9] A. Giri, P.E. Hopkins, A review of experimental and computational advances in thermal boundary conductance and nanoscale thermal transport across solid interfaces, Adv. Funct. Mater. 30 (2020), 1903857, https://doi.org/10.1002/adfm.201903857.

[10] M. Hu, Z. Yang, Perspective on multi-scale simulation of thermal transport in solids and interfaces, Phys. Chem. Chem. Phys. 23 (2021) 1785–1801, https://doi.org/10.1039/D0CP03372C.

[11] C. Monachon, G. Schusteritsch, E. Kaxiras, L. Weber, Qualitative link between work of adhesion and thermal conductance of metal/diamond interfaces, J. Appl. Phys. 115 (2014), 123509, https://doi.org/10.1063/1.4869668.

[12] L. Chen, S. Chen, Y. Hou, Understanding the thermal conductivity of diamond/copper composites by first-principles calculations, Carbon 148 (2019) 249–257, https://doi.org/10.1016/j.carbon.2019.03.051.

[13] H. Xie, Y. Chen, T. Zhang, N. Zhao, C. Shi, C. He, E. Liu, Adhesion, bonding and mechanical properties of Mo doped diamond/Al (Cu) interfaces: a first principles study, Appl. Surf. Sci. 527 (2020), 146817, https://doi.org/10.1016/j.apsusc.2020.146817.

[14] X. Shi, S. Huang, Y. Huang, Y. Zhang, S. Zong, S. Xu, Y. Chen, P. Ma, Atomic structures and electronic properties of Ni or N modified Cu/diamond interface, J. Phys-Condens. Mat. 32 (2020), 225001, https://doi.org/10.1088/1361-648X/ab686b.

[15] Y. Zhou, B. Anglin, A. Strachan, Phonon thermal conductivity in nanolaminated composite metals via molecular dynamics, J. Chem. Phys. 127 (2007), 184702, https://doi.org/10.1063/1.2802366.

[16] N. Khosravian, M.K. Samani, G.C. Loh, G.C.K. Chen, D. Baillargeat, B.K. Tay, Molecular dynamic simulation of diamond/silicon interfacial thermal conductance, J. Appl. Phys. 113 (2013), 024907, https://doi.org/10.1063/1.4775399.

[17] N. Yang, T. Luo, K. Esfarjani, A. Henry, Z. Tian, J. Shiomi, Y. Chalopin, B. Li, G. Chen, Thermal interface conductance between aluminum and silicon by molecular dynamics simulations, J. Comput. Theor. Nanos. 12 (2015) 168–174, https://doi.org/10.1166/jctn.2015.3710.

[18] Y. Tao, C. Liu, W. Chen, S. Cai, C. Chen, Z. Wei, K. Bi, J. Yang, Y. Chen, Mean free path dependent phonon contributions to interfacial thermal conductance, Phys. Lett. A 381 (2017) 1899–1904, https://doi.org/10.1016/j.physleta.2017.03.020.

[19] T. Feng, Y. Zhong, J. Shi, X. Ruan, Unexpected high inelastic phonon transport across solid-solid interface: modal nonequilibrium molecular dynamics simulations and Landauer analysis, Phys. Rev. B 99 (2019), 045301, https://doi.org/10.1103/PhysRevB.99.045301.

[20] D. Ma, L. Zhang, Enhancement of interface thermal conductance between Cr–Ni alloy and dielectric via Cu nano-interlayer, J. Phys-Condens. Mat. 32 (2020), 425001, https://doi.org/10.1088/1361-648X/aba014.

[21] M.H. Rahman, E.H. Chowdhury, M.R.B. Shahadat, M.M. Islam, Engineered defects to modulate the phonon thermal conductivity of Silicene: a nonequilibrium molecular dynamics study, Comp. Mater. Sci. 191 (2021), 110338, https://doi.org/10.1016/j.commatsci.2021.110338.

[22] D. Wu, H. Ding, Z. Fan, P. Jia, H. Xie, X. Chen, High interfacial thermal conductance across heterogeneous GaN/graphene interface, Appl. Surf. Sci. 581 (2022), 152344, https://doi.org/10.1016/j.apsusc.2021.152344.

[23] R.J. Stevens, L.V. Zhigilei, P.M. Norris, Effects of temperature and disorder on thermal boundary conductance at solid–solid interfaces: nonequilibrium molecular dynamics simulations, Int. J. Heat. Mass Transf. 50 (2007) 3977–3989, https://doi.org/10.1016/j.ijheatmasstransfer.2007.01.040.

[24] S. Fujii, K. Funai, T. Yokoi, M. Yoshiya, Grain-size dependence and anisotropy of nanoscale thermal transport in MgO, Appl. Phys. Lett. 119 (2021), 231604, https://doi.org/10.1063/5.0075854.

[25] X. Chen, K. Chen, Thermal transport of carbon nanomaterials, J. Phys. Condens. Mat. 32 (2020), 153002, https://doi.org/10.1088/1361-648X/ab5e57.

[26] P. Chantrenne, J.L. Barrat, Finite size effects in determination of thermal conductivities: comparing molecular dynamics results with simple models, J. Heat Transf. 126 (2004) 577–585, https://doi.org/10.1115/1.1777582.

[27] S. Plimpton, Fast parallel algorithms for short-range molecular dynamics, J. Comput. Phys. 117 (1995) 1–19, https://doi.org/10.1006/jcph.1995.1039.

[28] A. Stukowski, Visualization and analysis of atomistic simulation data with OVITO–the Open Visualization Tool, Model. Simulat. Mater. Sci. Eng. 18 (2009), 015012, https://doi.org/10.1088/0965-0393/18/1/015012.

[29] H. Huang, X. Tang, F. Chen, F. Gao, Q. Peng, L. Ji, X. Sun, Self-healing mechanism of irradiation defects in nickel–graphene nanocomposite: an energetic and kinetic perspective, J. Alloy. Compd. 765 (2018) 253–263, https://doi.org/10.1016/j.jallcom.2018.06.162.

[30] M.J. Demkowicz, R.G. Hoagland, Simulations of collision cascades in Cu–Nb layered composites using an EAM interatomic potential, Int. J. Appl. Mech. 1 (2009) 421–442, https://doi.org/10.1142/S1758825109000216.

[31] R. Devanathan, T. Diaz de la Rubia, W.J. Weber, Displacement threshold energies in β-SiC, J. Nucl. Mater. 253 (1998) 47–52, https://doi.org/10.1016/S0022-3115(97)00304-8.

[32] S.P. Huang, D.S. Mainardi, P.B. Balbuena, Structure and dynamics of graphite-supported bimetallic nanoclusters, Surf. Sci. 545 (2003) 163–179, https://doi.org/10.1016/j.susc.2003.08.050.

[33] X. Chen, X. Hu, P. Jia, Z. Xie, J. Liu, Tunable anisotropic thermal transport in porous carbon foams: the role of phonon coupling, Int. J. Mech. Sci. 206 (2021), 106576, https://doi.org/10.1016/j.ijmecsci.2021.106576.

[34] Z. Fan, P. Hirvonen, L.F.C. Pereira, M. Ervasti, K. Elder, D. Donadio, A. Harju, T. Ala-Nissila, Bimodal grain-size scaling of thermal transport in polycrystalline graphene from large-scale molecular dynamics simulations, Nano Lett 17 (2017) 5919–5924, https://doi.org/10.1021/acs.nanolett.7b01742.

[35] T. Liang, K. Xu, M. Han, Y. Yao, Z. Zhang, X. Zeng, J. Xu, J. Wu, Abnormally high thermal conductivity in fivefold twinned diamond nanowires, Mater. Today Phys. 25 (2022), 100705, https://doi.org/10.1016/j.mtphys.2022.100705.

[36] Z. Lu, A.M. Chaka, P.V. Sushko, Thermal conductance enhanced via inelastic phonon transport by atomic vacancies at Cu/Si interfaces, Phys. Rev. B 102 (2020), 075449, https://doi.org/10.1103/PhysRevB.102.075449.

[37] Z. Lu, N.P. Smith, M.P. Prange, R.A. Bunker, J.L. Orrell, A.M. Chaka, Effect of interfacial structures on phonon transport across atomically precise Si/Al

heterojunctions, Phys. Rev. Mater. 5 (2021), 086002, https://doi.org/10.1103/PhysRevMaterials.5.086002.
[38] H. Zou, Y. Feng, L. Qiu, Excellent heat transfer enhancement of CNT-metal interface by loading carbyne and metal nanowire into CNT, Int. J. Heat. Mass Transf. 186 (2022), 122533, https://doi.org/10.1016/j.ijheatmasstransfer.2022.122533.
[39] S.V. Kidalov, F.M. Shakhov, Thermal conductivity of diamond composites, Materials 2 (2009) 2467–2495, https://doi.org/10.3390/ma2042467.
[40] B. Xu, S.W. Hung, S. Hu, C. Shao, R. Guo, J. Choi, T. Kodama, F. Chen, J. Shiomi, Scalable monolayer-functionalized nanointerface for thermal conductivity enhancement in copper/diamond composite, Carbon 175 (2021) 299–306, https://doi.org/10.1016/j.carbon.2021.01.018.
[41] T. Zhang, S. Wu, R. Zheng, G. Cheng, Significant reduction of thermal conductivity in silicon nanowire arrays, Nanotechnology 24 (2013), 505718, https://doi.org/10.1088/0957-4484/24/50/505718.
[42] J. Al Hossain, B.H. Kim, Scale effects in the nanoscale heat transfer of molecular interfaces with different lattice orientations, AIP Adv. 11 (2021), 125311, https://doi.org/10.1063/5.0071760.
[43] L. Qiu, F. Li, N. Zhu, Y. Feng, Broad low-frequency phonon resonance for increased across-tube heat transport, Phys. Rev. B 105 (2022), 165406, https://doi.org/10.1103/PhysRevB.105.165406.
[44] H. Zou, Y. Feng, L. Qiu L, X. Zhang, Thermal conductance control of non-bonded interaction between loaded halogen molecules and carbon nanotubes: a molecular dynamics study, Int. J. Heat. Mass Transf. 183 (2022), 122216, https://doi.org/10.1016/j.ijheatmasstransfer.2021.122216.
[45] T. Liang, M. Zhou, P. Zhang, P. Yuan, D. Yang, Multilayer in-plane graphene/hexagonal boron nitride heterostructures: insights into the interfacial thermal transport properties, Int. J. Heat. Mass Tran. 151 (2020), 119395, https://doi.org/10.1016/j.ijheatmasstransfer.2020.119395.
[46] X. Wu, Q. Han, Semidefective graphene/h-BN in-plane heterostructures: enhancing interface thermal conductance by topological defects, J. Phys. Chem. C 125 (2021) 2748–2760, https://doi.org/10.1021/acs.jpcc.0c10387.
[47] Y. Jin, H. Huang, Y. Zhong, X. Yuan, H. Li, D. Lou, K. Xie, Z. Liu, B. Cai, Q. Peng, Role of interface on irradiation damage of Cu−diamond composites using classical molecular dynamics simulations, Ceram. Int. 48 (2022) 16813–16824, https://doi.org/10.1016/j.ceramint.2022.02.232.
[48] C. Zhang, H. Zhou, Y. Zeng, L. Zheng, Y. Zhan, K. Bi, A reduction of thermal conductivity of non-periodic Si/Ge superlattice nanowire: molecular dynamics simulation, Int. J. Heat. Mass Tran. 132 (2019) 681–688, https://doi.org/10.1016/j.ijheatmasstransfer.2018.12.041.
[49] Y. Hu, L. Zeng, A.J. Minnich, M.S. Dresselhaus, G. Chen, Spectral mapping of thermal conductivity through nanoscale ballistic transport, Nat. Nanotechnol. 10 (2015) 701–706, https://doi.org/10.1038/nnano.2015.109.
[50] M. Islam, I. Mia, S. Ahammed, C. Stampfl, J. Park, Exceptional in-plane and interfacial thermal transport in graphene/2D-SiC van der Waals heterostructures, Sci. Rep. 10 (2020) 1–16, https://doi.org/10.1038/s41598-020-78472-2.
[51] C. Liu, Q. Fu, Z. Gu, P. Lu, The reservoir area dependent thermal transport at the nanoscale interface, Phys. Chem. Chem. Phys. 22 (2020) 22016–22022, https://doi.org/10.1039/D0CP04001K.
[52] V. Samvedi, V. Tomar, The role of interface thermal boundary resistance in the overall thermal conductivity of Si–Ge multilayered structures, Nanotechnology 20 (2009), 365701, https://doi.org/10.1088/0957-4484/20/36/365701.
[53] X. Wu, Q. Han, Phonon thermal transport across multilayer graphene/hexagonal boron nitride van der waals heterostructures, ACS Appl. Mater. Inter. 13 (2021) 32564–32578, https://doi.org/10.1021/acsami.1c08275.
[54] P.G. Klemens, The scattering of low-frequency lattice waves by static imperfections, Proc. Phys. Soc. Sect. A 68 (1955) 1113–1128, https://doi.org/10.1088/0370-1298/68/12/303.
[55] J. Al-Ghalith, T. Dumitrică T, Nano-Scale Heat Transfer in Nanostructures: Toward understanding and Engineering Thermal Transport, Springer, Cham, 2018.
[56] M. Islam, I. Mia, A.S.M. Islam, C. Stampfl, J. Park, Temperature and interlayer coupling induced thermal transport across graphene/2D-SiC van der Waals heterostructure, Sci. Rep. 12 (2022) 1–15, https://doi.org/10.1038/s41598-021-04740-4.
[57] A. Cao, Molecular dynamics simulation study on heat transport in monolayer graphene sheet with various geometries, J. Appl. Phys. 111 (2012), 083528, https://doi.org/10.1063/1.4705510.
[58] V.T. Pham, T.H. Fang, Understanding porosity and temperature induced variabilities in interface, mechanical characteristics and thermal conductivity of borophene membranes, Sci. Rep. 11 (2021) 1–14, https://doi.org/10.1038/s41598-021-91705-2.
[59] G. Qin, Z. Qin, H. Wang, M. Hu, Anomalously temperature-dependent thermal conductivity of monolayer GaN with large deviations from the traditional 1/T law, Phys. Rev. B 95 (2017), 195416, https://doi.org/10.1103/PhysRevB.95.195416.
[60] A.S.M.J. Islam, M.S. Islam, N. Ferdous, J. Park, A.G. Bhuiyan, A. Hashimoto, Anomalous temperature dependent thermal conductivity of two-dimensional silicon carbide, Nanotechnology 30 (2019), 445707, https://doi.org/10.1088/1361-6528/ab3697.
[61] B. Hou, P. Liu, A. Wang, J. Xie, Interface optimization strategy for enhancing the mechanical and thermal properties of aligned graphene/Al composite, J. Alloy. Compd. 900 (2022), 163555, https://doi.org/10.1016/j.jallcom.2021.163555.
[62] T. Zhan, S. Minamoto, Y. Xu, Y. Tanaka, Y. Kagawa, Thermal boundary resistance at Si/Ge interfaces by molecular dynamics simulation, AIP Adv. 5 (2015), 047102, https://doi.org/10.1063/1.4916974.
[63] X. Wang, S. Shen, Effects of temperature and strain on thermal properties of Ni/Al laminated structure, Comp. Mater. Sci. 84 (2014) 13–17, https://doi.org/10.1016/j.commatsci.2013.11.037.
[64] A. Kandemir, A. Ozden, T. Cagin, C. Sevik, Thermal conductivity engineering of bulk and one-dimensional Si-Ge nanoarchitectures, Sci. Technol. Adv. Mat. 18 (2017) 187–196, https://doi.org/10.1080/14686996.2017.1288065.
[65] D. Liu, S. Wang, P. Yang P, Thermal property of graphene/silicon carbide heterostructure by molecular dynamics simulation, Acta Phys. Sin. 70 (2021), 187302, https://doi.org/10.7498/aps.70.20210613.